Available online at www.sciencedirect.com
ScienceDirect
Journal of the European Ceramic Society 29 (2009) 47–52
www.elsevier.com/locate/jeurceramsoc

3D analysis of crack morphologies in silicate glass using FIB tomography

F. Elfallagh *, B.J. Inkson

Department of Engineering Materials, The University of Sheffield, Mappin Street, Sheffield S1 3JD, United Kingdom

Received 8 February 2008; received in revised form 14 May 2008; accepted 17 May 2008
Available online 18 July 2008

Abstract

The surface damage and induced cracks around Vickers indents in soda-lime-silicate glass have been examined for the first time in 3D by cross-sectioning the indents using a highly focused ion beam (FIB). The 3D FIB tomographic analysis determines quantitatively both the location and 3D shape of individual cracks within a cluster around an indentation, and the 3D FIB technique will be applicable to analyse other types of surface damage in amorphous materials. For silicate glass it is shown that increasing the applied indent load from 50 to 200 g, results in a significant increase in measured crack density and 3D interconnections. It is also observed that the planar FIB cross-section surfaces cut through the very centre of the indents can undergo time-dependant strain and bulge outwards in order to relieve high local residual stresses.

Keywords: Glass; Indentation; Tomography; Cracks; FIB

1. Introduction

Soda-lime-silicate glasses are widely used as commercial glasses, for example as windows and glass containers. Silicate glasses are known to be brittle amorphous materials, and brittle fracture results from applied stresses.[1,2] The deformation of silicate glasses depends on many factors including composition, surface finish, environment, applied pressure, temperature and time.[1–4]

Plastic deformation at glass surfaces can be produced at room temperature by scratches and indentations using sharp or rounded punches at loads as small as 2 mN.[3–8] Loading with a sharp indenter like Vickers or Knoop diamonds typically results in a permanent plastic impression on the surface and a subsurface plastic deformation zone.[3,8,9] These residual damage zones contain a significant population of cracks with observed morphologies including radial, median, half-penny, and lateral cracks.[3,8,10] The system of cracks observed at a given indentation site depends on the material composition, environment, surface finish, indenter geometry, and peak contact load, and any, or all, of the main crack morphologies may be present for different combinations of these variables.[3]

The microstructure within the residual damage zones in glass have been analysed in 3D by a number of optical-based methods including confocal microscopy, optical imaging through the transparent material and imaging of serial sections obtained by acid dissolution of the surface.[7,11] These optical methods suffer from limitations in resolution making it difficult to image any but the biggest cracks in the 3D network.

It has been recently shown that the microstructural deformation and induced cracks around indents and scratches can be studied by cross-sectioning the localized damage site using a highly focused ion beam (FIB).[12–16] The 3D FIB tomography method involves milling serial cross-sections through a surface by FIB, imaging each sequential 2D section (typically by secondary electrons (SE)), and then aligning the 2D images of the sectioned material to reconstruct the 3D microstructure using specialized software (e.g. IMOD, IDL or Amira).[17]

In this work 3D FIB tomography has been applied for the first time to the analysis of subsurface damage beneath Vickers indentation sites in soda-lime-silicate glass. This enables the first direct measurement of the geometry and size of individual cracks within the damage zone. The 3D crack morphologies and densities obtained from the FIB tomographic analysis are compared for Vickers loads of 50, 100, and 200 g applied to the same material under identical indentation conditions. The

* Corresponding author.

0955-2219/$ – see front matter © 2008 Elsevier Ltd. All rights reserved.
doi:10.1016/j.jeurceramsoc.2008.05.042

results are discussed in light of possible artefacts arising from the invasive serial sectioning technique.

2. Experimental procedures

The glass used for these studies was standard commercially available soda-lime-silicate glass (Menzel-Glaser, Germany) of composition 14.30 wt% soda (Na_2O), 6.40 wt% lime (CaO) and 72.20 wt% silica (SiO_2). The samples were 1 mm thick and had a surface finish ≤ 1 μm.

2.1. Indentation procedure

A microhardness tester (Mitutoyo) was used to indent the glass sample under ambient conditions (24 °C, ~43% relative humidity) using a diamond Vickers indenter tip loaded to 50, 100 and 200 g and dwell time 15 s, keeping a constant tip and sample orientation between sequential indents.

2.2. Microstructural and FIB tomographic analysis

Samples were imaged and sputtered using a JSM 6500F SEM fitted with an Orsay Physics FIB column. The FIB-SEM samples were pre-coated with <20 nm of carbon to prevent charging and reduce ion beam damage. FIB trenches through the indentation sites were sputtered using 30 kV Ga^+ ions and beam currents of 50–250 pA. For 3D FIB tomography, the gallium focused ion beam was used at normal incidence to locally cross-section the indentation sites, and SEM secondary electron (SE) images were taken of each sequential x–y 2D slice at a tilt angle of 55° (see Fig. 1). The dimension of the 3D volume analysed for the 100 g indent site was $x = 25$ μm, $y = 8$ μm, $z = 22$ μm, total volume ~4400 μm^3, and for 200 g indent site the 3D volume was $x = 30$ μm, $y = 11$ μm, $z = 29$ μm, total volume ~9600 μm^3. To analyse these 3D volumes in a reasonable time, a microscope magnification of 3700–5000× was used, and the separation, z, of the 2D FIB sections was ~0.8 μm. The 2D SE images were aligned and corrected for drift using cross-correlation of features

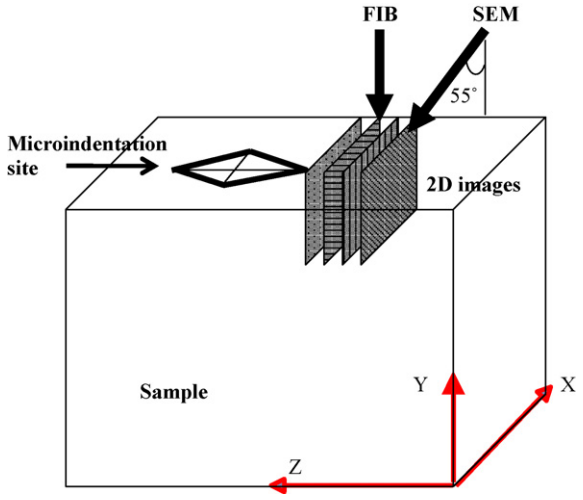

Fig. 1. Schematic of FIB serial sectioning geometry.

on the surfaces of the sample.[14–16] Cracks were identified and traced in each 2D section, and a mesh was generated to interpolate between sequential sections and display the analysed 3D volume using IMOD software.[17–19]

3. Results and discussion

3.1. Microindentation of silicate glass

The residual damage at the Vickers indentation sites, loads 50, 100 and 200 g with identical diamond tip and crystal orientation, was imaged by SEM at 15 kV. The Vickers hardness of the silicate glass sample under ambient conditions (24 °C, ~43% relative humidity) was found to be 5.55 GPa ± 2% averaged over four indents, which is within the expected range, e.g. the reported value of 5.9 GPa.[3] Imaged after fifteen days of indentation, the 50 g indent sites did not show any observable radial cracks (Fig. 2(a)), in contrast to 100 and 200 g sites where radial and circumferential cracks were observed in increasing density (Fig. 2(b and c)). The depths of residual damage craters were measured to be ~3.7 μm for the 100 g indent sites and ~5.25 μm for the 200 g sites.

Fig. 2 shows the two types of cracks visible on the surface around these indentation sites, namely (i) radial cracks, and (ii) circumferential cracks.[3,7,20,21] Most of the 100 g indent sites showed only three radial cracks, of maximum length 12 μm, which connect to the outermost circumferential cracks. The higher load 200 g sites showed four radial cracks of maximum length 25 μm eminating from the corners of the residual indent impression (Fig. 2(b and c)). In brittle materials radial cracks typically initiate near the edges of the Vickers indenter tips where there is the highest stress concentration.[3,22] Some of the radial cracks in this study showed a small surface offset from the corners of the residual indent impression, which may arise when cracks nucleate subsurface and deviate as they propagate upwards towards the free surface.[3]

The surface observations of the cracks around the Vickers indentations in silicate glass (Fig. 2) are consistent with those previously reported in other comparable studies.[3,7,20,21] In addition to the cracks, a spidery zone of light grey contrast was also observed to surround the residual damage zone and surface cracks (Fig. 2). This effect was only observed on specimens with a carbon coating. It appears to originate from microstructural changes of the carbon film due to topographic changes at the indentation site occurring after the C-film was deposited. Silicate glasses are known to be viscoelastic materials, and time-dependant changes at the indentation site to reduce stress are discussed further in Section 3.3.

3.2. 3D FIB tomography of cracks around Vickers microindentations in glass

The significant number of cracks which nucleate and propagate to relieve the high local stresses generated during the indentation process form a complex 3D network. FIB tomography can be used to characterise in 3D highly localized surface

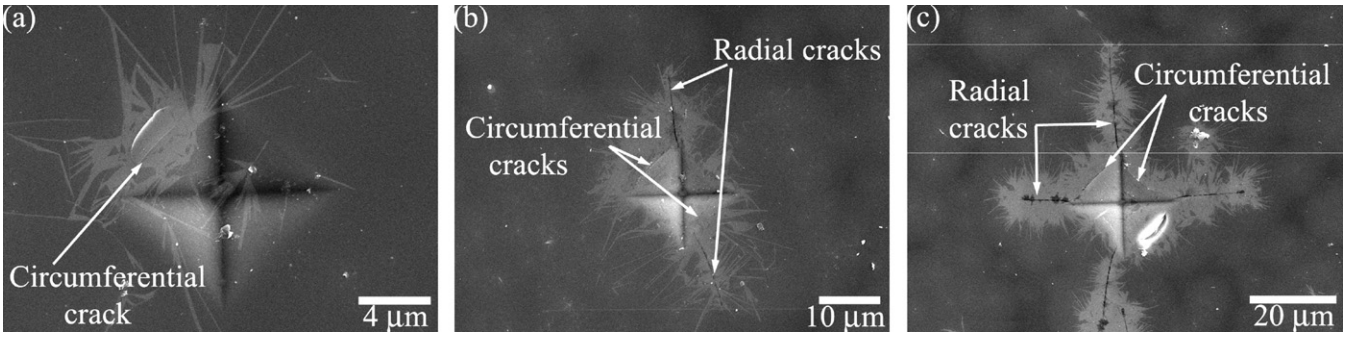

Fig. 2. SE images of Vickers indentation sites in silicate glass with radial and circumferential crack patterns. (a) 50 g load. (b) 100 g load. (c) 200 g load. The depths of the residual damage crater are ~3.7 μm for the 100 g site and ~5.25 μm for the 200 g site.

damage such as from indents and scratches,[12–14] and FIB tomography is applied here for the first time to quantitatively analyse the 3D crack distribution in silicate glass.

3.2.1. Subsurface crack analysis

Deep trenches ~25 μm wide and 8–11 μm deep were sputtered by FIB on one side of the Vickers microindentations aligned symmetrically with (and parallel to) one of the diagonals (Fig. 1). The specimen volume containing the indent was then serially sectioned, taking a 2D SE image of each new cross-sectional surface to image the crack distribution. Fig. 3 shows typical images of cracks observed underneath the residual indent impression for 100 and 200 g Vickers microindentations.

Two major crack systems, circumferential and median cracks, were observed beneath the 100 g indentation site in glass (Fig. 3(a and b)). The median crack extended deep into the material to maximum depth of >9 μm, connecting to the surface at two opposite radial crack positions forming a so-called a semi-elliptical shape crack (see Fig. 4,[7,23]). At the centre of the indent, the median crack remained subsurface, remaining below the central plastically deformed deformation zone (Fig. 3(b)). The same median crack system was observed beneath the 200 g site except that the median crack was connected to three radial cracks, i.e. one radial at one corner of the residual indent impression and a radial and a branching secondary radial on the opposite side of the indentation site (Fig. 3(c)).

The major cracks observed in the 2D FIB sections appeared to have a wider profile than that observed at the top surface prior to sectioning, indicating some crack opening at the new free surface due to the removal of the confining material. In some of the 2D FIB cross-sections it was also observed that the SE contrast varied across some of the new FIB-cut free surfaces (Fig. 3). This appears to be due to topographic SE contrast arising from some bulging of the material to relieve residual stress, especially in the areas of the new free surfaces furthest from cracks and boundaries (Fig. 3). This effect is discussed further in Section 3.3.

3.2.2. 3D tomographic reconstructions of crack distribution under indents

3D tomographic maps of the subsurface cracks under the indent sites were generated from multiple 2D cross-sections using IMOD software.[17] Fig. 4 shows the 3D reconstructions from 21 sections through a 100 g indent site and 14 sections through a 200 g indent site. The main features of the observed 3D crack distributions are:

i. An increasing crack density observed with increasing indentation load. 2 major cracks can be clearly identified under the 100 g indent and 6 major cracks under the 200 g indent site.
ii. Median-radial cracks occurring perpendicular to the surface beneath the indentation site corners, and running under the centre of residual plastically deformed zone with orientation deviating by ~20° from the vertical plane to form a semi-elliptical crack shape. The maximum depth of this crack for the 100 g indent is >9 μm, with crack surface area >160 μm^2.
iii. Circumferential cracks, the outermost being inclined to the original surface plane by ~30°. The major circumferential crack observed at the 100 g indent site had maximum depth

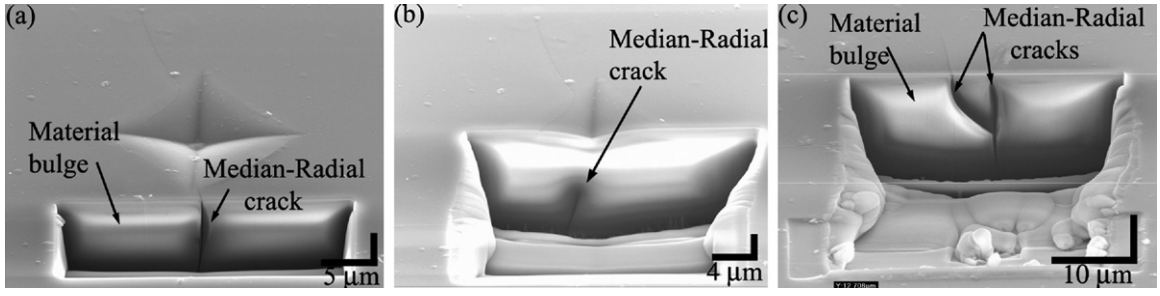

Fig. 3. SE images of FIB cross-sections through Vickers indentation residual damage zones in soda-lime-silicate glass. (a) 100 g indent site after first section. (b) 100 g indent site sectioned through the centre (c) 200 g indent site after 14 sections, with complete removal of the residual indent impression.

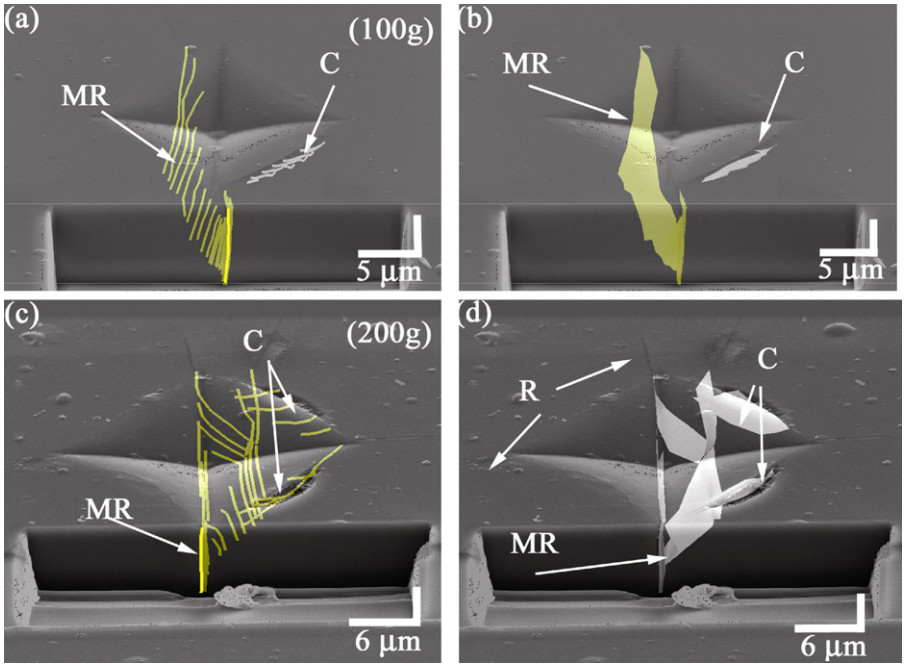

Fig. 4. 3D FIB tomographic maps of crack distributions under (a and b) 100 g and (c and d) 200 g Vickers indentation sites, viewing angle 55°, where R, C and MR indicate radial, circumferential and median-radial cracks. (a and c) Crack maps without mesh. (b and d) Crack maps with a mesh connecting sequential 2D sections, overlaid with an image of the specimen geometry.

~2 μm (Fig. 4(a and b)). The circumferential cracks for the 200 g indent propagated further towards the indent centre and linked up with the median and radial crack system (Fig. 4(c and d)).

The process of FIB tomographic sectioning can have an invasive effect on the observed crack distribution due to microstructural changes induced by sputtering and stress changes.[12,13,24] A significant feature of the 3D FIB tomographic analysis of the cracks in glass is that the density of circumferential cracks observed on the surface of the sample (by SEM, Fig. 2) is higher that the crack density observed beneath the indentation site (Figs. 3 and 4). This effect, also seen in FIB tomography of indents in alumina,[24] may arise (1) due to there being a size threshold for crack observation, possibly due to FIB sputtering of material into the finest cracks masking their presence, and/or (2) that the FIB sectioning procedure is resulting in some minor crack closure due to stress changes.

FIB tomography induces local changes in the residual stress state of the material being examined.[24] The change of stress is both a function of the geometry of the FIB-sputtered trenches cut into the material, and their location with respect to the pre-existing microstructure and residual stress state of the sample, for example proximity to the central residual plastic damage zone of an indent.[12,24] In alumina it has been observed that the removal of the highly stressed central residual plastic damage zone of the indent during FIB tomography results in a reduction in both the residual stress and observed crack density in the remaining material.[24] For the silicate glass indents examined here, only a very small number of cracks to relieve stress were observed in the 2D FIB cross-sections through the Vickers indents compared to alumina samples indented with the same applied load. The residual stress existing in the indented glass was observed to drive time-dependant viscoelastic creep, discussed in the next section.

3.3. Stress relief in silicate glass at indentation sites

The indentation of the silicate glass results in a zone of residual plastic deformation and stress. Silicate glasses are known to be viscoelastic, and it is expected that a significant residual stress field can drive material diffusion over time, leading to local stress relaxation and viscoelastic creep.[25] Here it is observed that ultrathin carbon films deposited over indentation sites undergo detectable contrast changes in the vicinity of the residual indent impressions and associated surface cracks (Section 3.1, Fig. 2). This appears to be driven by post-indentation topology changes within the deformation zone. SEM images of similar silicate glass samples which have been indented and then annealed to reduce the residual stress before carbon coating do not show this effect, as expected with no significant stress field to drive time-dependant strain.

The process of cutting a FIB trench into the indented glass to enable FIB tomography enables residual stress to be relieved at the new free surface. There is some evidence that existing cracks can open up at the new free surface (Fig. 3). Perhaps more dramatic is the strong SE contrast variations observed at the 2D FIB cross-sections cut through the deformation zones (Fig. 3). Similar zones of bright SE contrast have also been observed under alumina indents.[24] Here, the contrast appears to arise from topographic SE contrast due to rapid deformation of the glass outwards from the FIB-cut plane especially in the areas of the new free surfaces furthest from cracks and boundaries (Fig. 3(b)). The bulging of material to relieve residual com-

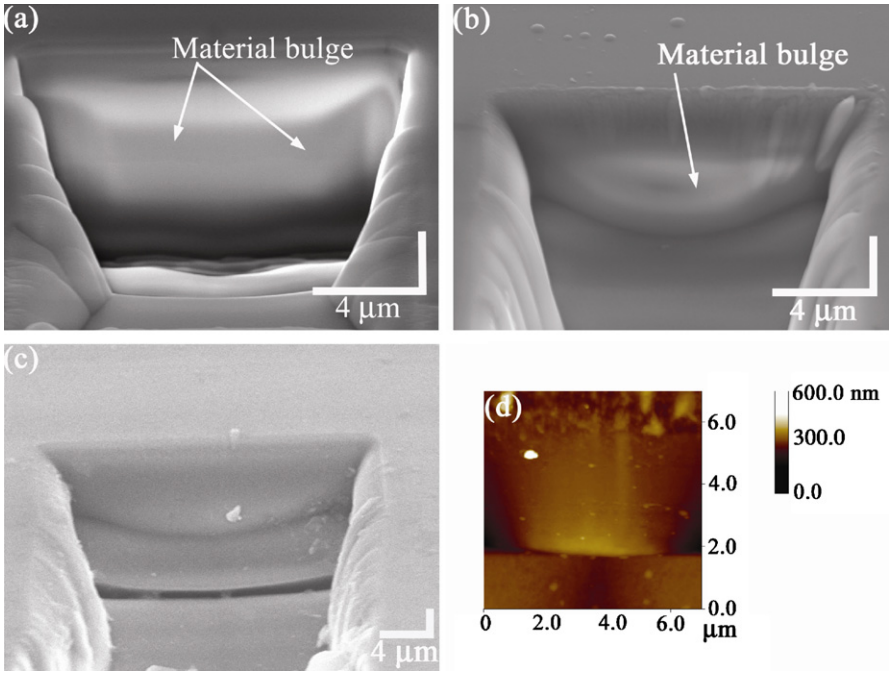

Fig. 5. SE images of material bulges at FIB cross-sections through indents in silicate glass. (a) 50 g indentation imaged immediately after FIB sputtering (b) FIB section in (a) after 3 weeks showing viscoelastic flow. (c) Material bulge at a 2D FIB section through a 100 g Vickers indentation site. (d) AFM image of the mid area of the same 2D section in (c).

pressive stress was observed on FIB cross-sections through the centres of all 50, 100 and 200 g silicate glass indents.

Fig. 5(a) shows the bulging of material at a FIB cross-sectional surface through a 50 g indent site directly after milling the FIB trench. The same FIB trench was imaged 3 weeks later (Fig. 5(b)), where it can be seen that significant time-dependent strain (viscoelastic creep) has occurred to reduce the local residual stress further, causing growth of the bulge. The existence of the bulges in big FIB trenches can be confirmed by AFM (Fig. 5(c and d)).

The immediate and viscoelastic displacement of the silicate glass at the FIB-cross-sections is a function of the local residual stress field. For a given FIB cross-section, the maximum displacement of the glass at any given time occurred about 2–5 μm below the original free surface of the specimen, corresponding to the maximum compressive stress zone. The displacement also increased with distance from any cracks (which reduce stress, Fig. 3(b)) and the side and bottom restraining walls of the FIB trench. The bulging of the material could be significantly reduced by annealing the glass sample after indentation to reduce the residual stress. Fig. 6 shows a FIB cross-section through a 50 g indent after annealing at 550 °C in an argon environment for 1 h before FIB sectioning. The material relaxation at the new FIB-cut free surface, and hence associated topographic SE contrast, has been drastically reduced compared to the as-indented 50 g sample (Figs. 5(a) and 6).

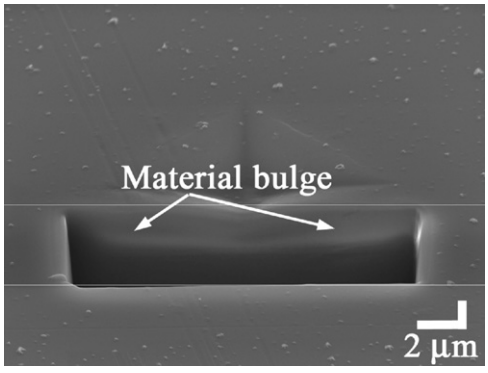

Fig. 6. SE image of a FIB cross-section through a 50 g indent on silicate glass annealed at 550 °C for 1 h, showing reduced material bulging due to stress compared to an un-annealed indent (Fig. 5(a)).

4. Conclusions

Crack morphologies around Vickers microindentations in soda-lime-silicate glass samples have been analysed in 3D using FIB tomography. It is shown that:

- The location and 3D shape of individual cracks in silicate glass, including radial, median and circumferential cracks within a cluster around an indentation, can be quantitatively determined.
- There is a systematic increase in measured crack density and 3D interconnection resulting from Vickers indents in silicate glass as the load increases 50 g → 100 g → 200 g.
- Semi-elliptical cracks, resulting from subsurface medians joining to radials, were observed beneath indentation sites at 100 g and 200 g loads. The orientation of these cracks deviated by up to ∼20° from the vertical below the residual plastic zone.

- Time-dependant strain of silicate glass was observed at FIB-sputtered free surfaces cut through the residual compressive stress zones under the indent sites.
- The viscoelastic material displacement at the FIB trenches can be significantly reduced by annealing the glass to reduce the local residual stresses.

It is concluded that FIB tomographic analysis is a useful technique to investigate the major features of the crack distribution around indents and surface wear in silicate glass. The major crack morphologies are consistent with those identified via optical and 2D electron microscopy methods.[3,25] The 3D FIB tomography technique gives the added benefit of characterising quantitively the 3D shape and size of individual cracks and crack networks at high spatial resolution, and at a surface location that can be chosen with <100 nm spatial resolution.

However it is also observed that the FIB tomography technique must be applied with great care in glasses. FIB sputtering causes changes in residual stress close to FIB trenches.[24] During FIB tomography of silicate glass, relaxation of stress can generate time-dependant bulging of material at the FIB cross-sections, which increases with time after the FIB processing due to viscoelastic creep. For the case of analysis of Vickers microindentations in glass, this material relaxation can be reduced by annealing the sample prior to the FIB tomographic sectioning.

Acknowledgements

F. Elfallagh acknowledges the financial support of Ministry of Higher Education of Libya.

The authors thank Dr. Russell J. Hand for discussions.

References

1. Bridgman, P. W. and Simon, I., Effects of very high pressures on glass. *Appl. Phys.*, 1953, **24**, 405–413.
2. Sakka, S. and Mackenzie, J. D., High pressure effects on glass. *Non-Cryst. Solids*, 1969, **1**, 107–142.
3. Cook, R. F. and Pharr, G. M., Direct observation and analysis of indentation cracking in glasses and ceramics. *Am. Ceram. Soc.*, 1990, **73**, 787–817.
4. Sglavo, V. M. and Green, D. J., Subcritical growth of indentation median cracks in soda-lime-silica glass. *Am. Ceram. Soc.*, 1995, **78**, 650–656.
5. Marsh, D. M., Plastic flow in glass. *Proc. R. Soc. Lond. Ser. A, Math. Phys. Sci.*, 1964, **279**, 420–435.
6. Woirgard, J., Tromas, C., Girard, J. C. and Audurier, V., Study of the mechanical properties of ceramic materials by nanoindentation technique. *Eur. Ceram. Soc.*, 1998, **18**, 2297–2305.
7. Whittle, B. and Hand, R., Morphology of vickers indent flaws in soda-lime-silica glass. *Am. Ceram. Soc.*, 2001, **84**, 2361–2365.
8. Sglavo, V. M. and Green, D. J., The sub-critical indentation fracture process in sods-lime-silica glass. *Eng. Fact. Mech.*, 1996, **55**(1), 35–46.
9. Ziemath, E. C. and Herrmann, P. S., Densification and residual stresses induced in glass surfaces by Vickers indentation. *Non-Cryst. Soilds*, 2000, **273**, 19–24.
10. Wiederhorn, S. M. and Lawn, B. R., Strength degradation of glass resulting from impact with spheres. *Am. Ceram. Soc.*, 1977, **60**, 451–458.
11. Michel, M. D., Mikowski, A., Lepienski, C. M., Foerster, C. E. and Serbena, F. C., High temperature microhardness of soda-lime glass. *Non-Cryst. Solids*, 2004, **348**, 131–138.
12. Inkson, B. J., Leclere, D., El Fallagh, F. and Derby, B., The effect of focused ion beam machining on residual stress and crack morphologies in Alumina. *Phys. Conf. Ser.*, 2006, **26**, 219–222.
13. Inkson, B. J., Wu, H. Z., Steer, T. J. and Möbus, G., 3D mapping of subsurface cracks in alumina using FIB Fundamentals of nanoindentation and nanotribology. *Proc. Mater. Res. Soc.*, 2001, **649**, Q7.7.1–Q7.7.6.
14. Wu, H. Z., Roberts, S. G., Möbus, G. and Inkson, B. J., Subsurface damage analysis by TEM and 3D FIB crack mapping in alumina/5 vol.%SiC nanocomposites. *Acta Mater.*, 2003, **51**, 149–163.
15. Inkson, B. J., Steer, T., Möbus, G. and Wagner, T., Subsurface nanoindentation deformation of Cu–Al multilayers mapped in 3D by focused ion beam microscopy. *Microscopy*, 2001, **201**(Pt 2), 256–269.
16. Steer, T. J., Möbus, G., Wagner, T., Kraft, O. and Inkson, B. J., 3D FIB mapping of nanoindentation zones in a Cu–Ti multilayered coating. *Thin Solid Films*, 2002, **413**, 147–154.
17. Kremer, J. R., Mastronarde, D. N. and McIntosh, J. R., Computer visualization of three-dimensional image data using IMOD. *Struct. Biol.*, 1996, **116**, 71–76.
18. Groeber, M. A., Haley, B. K., Uchic, M. D., Dimiduk, D. M. and Ghosh, S., 3D reconstruction and characterization of polycrystalline microstructures using a FIB-SEM system. *Mat. Charac.*, 2006, **57**, 259–273.
19. Ma, L. W., Cairney, J. M., McGrouther, D., Hoffman, M. and Munroe, P. R., Three dimensional imaging of deformation modes in TiN-based thin film coatings. *Thin Solid Films*, 2007, **515**, 3190–3195.
20. Burghard, Z., Zimmermann, A. and Rödel, J., Crack opening profiles of indentation cracks in normal and anomalous glasses. *Acta Mater.*, 2004, **52**, 293–297.
21. Wilantewicz, T. E. and Varner, J. R., Vickers indentation behaviour of several commercial glasses at high temperature. *Mater. Sci.*, 2008, **43**, 281–298.
22. Guillou, M. O., Henshall, J. L. and Hooper, R. M., Indentation fracture and soft impresser fatigue in sapphire and polycrystalline alumina. *Refractory Metals Hard Mater.*, 1998, **16**, 323–329.
23. Sglavo, V. M., Gadotti, M. and Micheletti, T., Cyclic loading behaviour of soda-lime-silicate glass using indentation cracks. *Fatigue Fract. Eng. Mat. Struct.*, 1997, **20**, 1225–1234.
24. Elfallagh, F. and Inkson, B. J., Evolution of residual stress and crack morphologies during 3D FIB tomographic analysis of alumina. *Microscopy*, 2008, **230**, 240–251.
25. Le Bourhis, E. and Metayer, D., Indentation of glass as a function of temperature. *Non-Cryst. Solids*, 2000, **272**, 34–38.